NASA/TM–2011-217049

Evaluation of Long Composite Struts

Dawn C. Jegley and K. Chauncey Wu
Langley Research Center, Hampton, Virginia

James E. Phelps and Martin J. McKenney
ATK Space Systems, Inc., Hampton, Virginia

Leonard Oremont
Lockheed Martin, Hampton, Virginia

Ansley Barnard
University of Washington, Seattle, Washington

February 2011

NASA STI Program . . . in Profile

Since its founding, NASA has been dedicated to the advancement of aeronautics and space science. The NASA scientific and technical information (STI) program plays a key part in helping NASA maintain this important role.

The NASA STI program operates under the auspices of the Agency Chief Information Officer. It collects, organizes, provides for archiving, and disseminates NASA's STI. The NASA STI program provides access to the NASA Aeronautics and Space Database and its public interface, the NASA Technical Report Server, thus providing one of the largest collections of aeronautical and space science STI in the world. Results are published in both non-NASA channels and by NASA in the NASA STI Report Series, which includes the following report types:

- TECHNICAL PUBLICATION. Reports of completed research or a major significant phase of research that present the results of NASA programs and include extensive data or theoretical analysis. Includes compilations of significant scientific and technical data and information deemed to be of continuing reference value. NASA counterpart of peer-reviewed formal professional papers, but having less stringent limitations on manuscript length and extent of graphic presentations.

- TECHNICAL MEMORANDUM. Scientific and technical findings that are preliminary or of specialized interest, e.g., quick release reports, working papers, and bibliographies that contain minimal annotation. Does not contain extensive analysis.

- CONTRACTOR REPORT. Scientific and technical findings by NASA-sponsored contractors and grantees.

- CONFERENCE PUBLICATION. Collected papers from scientific and technical conferences, symposia, seminars, or other meetings sponsored or co-sponsored by NASA.

- SPECIAL PUBLICATION. Scientific, technical, or historical information from NASA programs, projects, and missions, often concerned with subjects having substantial public interest.

- TECHNICAL TRANSLATION. English-language translations of foreign scientific and technical material pertinent to NASA's mission.

Specialized services also include creating custom thesauri, building customized databases, and organizing and publishing research results.

For more information about the NASA STI program, see the following:

- Access the NASA STI program home page at *http://www.sti.nasa.gov*

- E-mail your question via the Internet to help@sti.nasa.gov

- Fax your question to the NASA STI Help Desk at 443-757-5803

- Phone the NASA STI Help Desk at 443-757-5802

- Write to:
  NASA STI Help Desk
  NASA Center for AeroSpace Information
  7115 Standard Drive
  Hanover, MD 21076-1320

NASA/TM–2011-217049

Evaluation of Long Composite Struts

Dawn C. Jegley and K. Chauncey Wu
Langley Research Center, Hampton, Virginia

James E. Phelps and Martin J. McKenney
ATK Space Systems, Inc., Hampton, Virginia

Leonard Oremont
Lockheed Martin, Hampton, Virginia

Ansley Barnard
University of Washington, Seattle, Washington

National Aeronautics and
Space Administration

Langley Research Center
Hampton, Virginia 23681-2199

February 2011

Available from:

NASA Center for AeroSpace Information
7115 Standard Drive
Hanover, MD 21076-1320
443-757-5802

Evaluation of Long Composite Struts

Dawn Jegley, K. Chauncey Wu
NASA Langley Research Center, Hampton VA

James Phelps, Martin McKenney
ATK Space Systems, Inc., Hampton VA

Leonard Oremont
Lockheed Martin, Hampton VA

Ansley Barnard
University of Washington, Seattle WA

Carbon-epoxy tapered struts are structurally efficient and offer opportunities for weight savings on aircraft and spacecraft structures. Seven composite struts were designed, fabricated and experimentally evaluated through uniaxial loading. The design requirements, analytical predictions and experimental results are presented. Struts with a tapered composite body and corrugated titanium end fittings successfully supported their design ultimate loads with no evidence of failure.

I. Introduction

NASA evaluates the efficiency of structural concepts for aircraft and spacecraft components with the goal of designing lightweight parts. Currently NASA is interested in structurally efficient truss structures for application to spacecraft and aircraft components such as supports for antennae or solar panels, lunar lander struts, components for use on the lunar surface, strut-braced wing components, aircraft spars or unmanned aerial vehicles.

Structural efficiency is defined here as the ratio of a structure's load-carrying ability to its mass. Studies involving the structural efficiency of shells date back to the NACA days and are continued into aircraft design today.[1-7] Composite materials and non-traditional designs offer opportunities for reduced mass compared to conventional aluminum tubes with a uniform circular cross section. An example of a structure dependent upon struts in the truss arrangement is the Altair lunar lander[8] as shown in Fig. 1. The Altair project is one element of NASA's Constellation program, which is intended to return human's to the Moon within approximately the next 10-15 years. Because of the need to reduce mass, the lunar lander truss elements must be designed to operate at maximum efficiency. The use of composite struts to directly carry propellant and payload induced launch loads is generally speaking unique. Long struts have been evaluated in the context of deployable parts of a space station, telescope elements, and solar panels. In general, these applications require precise positioning but carry little load and tend to be driven by stiffness rather then strength requirements. In contrast, some of the struts for Altair must carry loads greater than 100,000 lb.[8] Therefore, the primary focus of this study is heavily loaded struts, although several lightly-loaded strut designs are discussed as well.

The struts in the current study involve predicted maximum loads ranging from 1,260 lb to 129,998 lb. Struts were designed to a specified Design Ultimate Load (DUL) with a 1.4 safety margin with respect to strength, Euler buckling, and local buckling so 1.4 was used as the margin to determine Design Limit Load (DLL). Detailed discussions of the design, optimization and fabrication of the struts discussed herein is presented in references 9-14. The focus of the current paper is the experimental behavior and a comparison to the finite element analysis of each strut. Two struts fabricated by Boeing and five struts fabricated by Northrop Grumman were evaluated experimentally while subjected to uniaxial loading. Results of these experiments are described in the following sections.

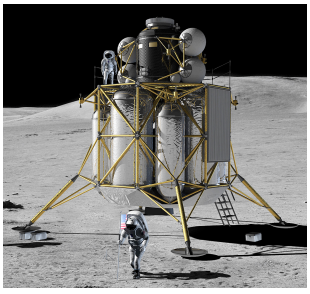

Figure 1. Altair lunar lander.

II. Test Article Description

All struts were fabricated using IM7-977-3 or IM7-8552 carbon fibers and epoxy resin and titanium end fittings. Each strut consists of a composite tube body and a titanium end fitting on each end. Two types of struts were considered. The Northrop Grumman struts contained a composite body-to-fitting joint in which the fibers were wrapped around the corrugations in the titanium and the other Boeing struts contained a step-joint fitting where the titanium was bonded to the composite. Struts with the corrugated end fitting had a composite body with a wider diameter in the center and small diameter on the end. Struts with the step-lap joint bonded fitting had a uniform diameter body and a tapered titanium fitting.

Seven full-scale, optimum-design, test articles were fabricated based on designs developed in references 12 and 13. Photographs of representative test articles are shown in Fig. 2. Struts designed to support a compressive DUL of 107,845 lb are shown in Figs. 2a and 2b. A strut designed to support a compressive DUL of 1,182 lb is shown in Fig 2c. Struts shown in Figs. 2a and 2c have corrugated end fittings and the strut shown in Fig. 2b has a bonded end fitting. Photographs of typical fittings (prior to strut fabrication) are shown in Fig. 3. Descriptions of the composite struts are shown in Table 1. A sketch of a strut with the definitions of the dimensions used in Table 1 is shown in Fig. 4. All fittings contained internal threads to match the test fixtures.

a) Heavily loaded Northrop Grumman strut.

b) Heavily loaded Boeing strut.

c) Lightly loaded Northrop Grumman strut.

Figure 2. Strut test articles.

Strut types are identified herein by their designer (B for Boeing and N for Northrop Grumman) and their load level (L for lightly loaded struts and H for heavily loaded struts). Additionally, a replicate number of 1,2, or 3 is added to differentiate individual struts within a type.

Figure 3. Titanium fittings.

Table 1. Strut Description

Strut type	Qty	Strut Length (in.), L	Central Inner Diameter (in.), D	Central Stacking Sequence %0/%45/%90	Composite Untapered Length (in.), b	Taper Location, Angle, α	Fitting Length (in.), f	Fitting Concept*
B-H	2	77.7	5.8	63/25/12	61.0	Fitting, 22°	8.35	Bond
N-H	3	77.7	6.0	58/24/18	50.7	Body, 10°	2.94	Cor.
N-L	2	100.3	2.0	33/44/22	92.7	Body, 10°	1.25	Cor.

* Cor.=corrugated; Bond=bonded

The composite strut bodies of the heavily loaded struts contained 16 and 18 plies with stacking sequences $[\pm 45/0_3/90/0_2]_s$ for struts B-H and $[90/0_2/\pm 45/0_3/90]_s$ for struts N-H. B-H and N-H struts were designed to support an axial compressive DUL of 107,585 lb and an axial tensile DUL of 60,182 lb. The composite strut bodies for the lightly loaded struts contained nine plies with a stacking sequence of $[90/0/\pm 45/\overline{0}]_s$ and were designed to support 1,183 lb in compression and 1,443 lb in tension. Additionally,

several extra 90° plies were added to a small region of the N-L and N-H struts around the outermost end of the taper, as shown in Fig. 4. These additional wraps were applied to reduce the stress concentration in that region without adding another ply along the whole length of the strut.

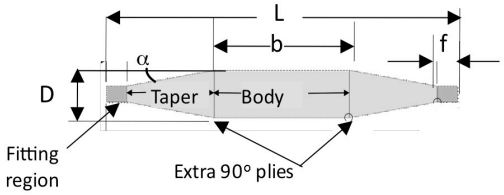

Figure 4. Reinforcement at taper edge.

The struts with the tapered body and the corrugated end fittings, N-H and N-L, had the end-most fibers wound around the corrugations in the fitting to create a mechanical joint as well as curing the part with the fitting in place to create an adhesive bond. The corrugated fitting concept has a series of grooves in the outer surface of the fitting which allow fibers to be placed into the groves and overwrapped with additional fibers which lock the layers in place. After the strut is cured, the fibers are locked into the grooves and the fitting cannot be removed solely by breaking the adhesive bond. The only way to fail this joint is to break the fibers themselves. The geometry of the fitting is dependent upon the design load levels. Details of the manufacturing approach are presented in reference 12.

The composite portion of the struts of type B-H, which have a uniform diameter body and tapered end fittings, were fabricated with dropped plies on each end to create steps of reduced numbers of plies. The machined titanium fittings were bonded to the dropped-ply region to allow an adhesive bond to hold the fittings in place. The bonded fitting concept uses a lap-stepped joint and adhesive to attach the titanium fitting to the carbon-epoxy during cure. When the bonded fitting was used, the taper was in the fitting rather than in the composite so a much steeper taper angle was achieved than could be fabricated in a composite body taper. However, a longer fitting was required to gain adequate bond area. Details of manufacturing approach are presented in reference 13.

Geometric imperfection evaluations for all struts were conducted either by the contractor who did the fabrication or by NASA. The only imperfection shape considered herein is a single half-wave deformation as shown in the sketch in Fig. 5. The measured imperfection amplitudes for each strut are shown in Table 2.

Table 2. Measured Geometric Imperfections

Strut ID	Measured imperfection amplitude (in.)	
	NASA measurement	Contractor measurement
N-L-1	0.020	0.029
N-L-2	0.031	0.012
B-H-1	0.020	0.004
B-H-2	0.020	0.004
N-H-1	0.006	0.0043
N-H-2	0.034	0.225
N-H-3	0.025	0.023

III. Analysis

All fabricated struts were analyzed using the finite element code ABAQUS[16] to determine the buckling load, strain distribution and failure load. Linear analyses indicated that none of the struts would fail in the composite body in tension due to excessive strains at loads less than DUL. However, additional factors beyond strains had to be considered for compression. In each compression analysis an imperfection shape of one axial half-wave was assumed, as shown in Fig. 5. The largest measured imperfection was used as the wave's amplitude in the nonlinear analysis.

A typical finite element model is shown in Fig. 6. Between 10,000 and 70,000 shell elements were used in each model. The properties of carbon-epoxy and titanium, as shown in Table 3, were used for the analysis. Pinned boundary conditions were implemented by adding multi-point constraints to attach each node at the end of the strut to a single load application point. These constraints are indicated by the pink connectors in Fig. 6. This load application point was located three to six inches from

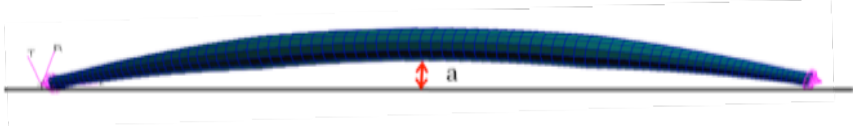

Figure 5. Shape of initial geometric imperfection.

the end of the strut. Displacements and rotations were constrained at this point to avoid convergence difficulties in the analysis. This pinned condition is assumed to be conservative since the actual hardware is more rigid than a true pinned condition but not as rigid as a clamped condition. Load-displacement and load-strain relationships were predicted for all struts to guide testing. Detailed analyses of the fittings and the fitting-composite interface were conducted during the design process and are presented in references 12 and 13, but are not presented herein. Predictions of maximum loads for each strut type are shown in Table 4. Bifurcation buckling loads were calculated with no assumed imperfections while maximum predicted loads were calculated based on the assumed imperfection.

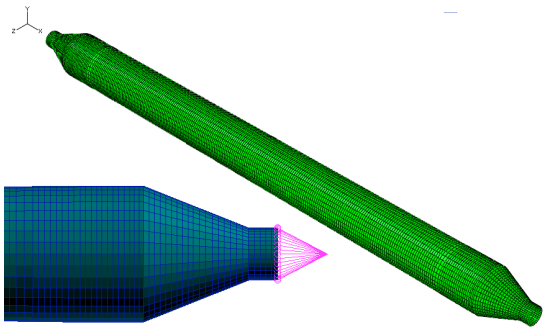

Figure 6. Typical finite element model.

Table 3. Assumed Material Properties

	Carbon-epoxy Compression	Carbon-epoxy Tension	Titanium Tension and Compression
E_{11}, psi	21,400,000	24,500,000	16,000,000
E_{22}, psi	1,460,000	1,260,000	16,000,000
G_{12}, psi	690,000	690,000	6,060,610
ν_{12}	0.3	0.3	0.32

Table 4. Analytical Predictions

Strut Type	Required Compressive DUL (lb)	Required Tensile DUL (lb)	Predicted Bifurcation Buckling Load (lb)	Predicted Maximum Load (lb)	Assumed Imperfection Amplitude (in.)
B-H	107,585	60,182	121,600	113,804	0.020
N-H	107,585	60,182	141,700	129,998	0.043
N-L	1,183	1,443	1,290	1,260	0.029

IV. Specimen Preparation and Testing

Between twenty and forty strain gages were attached to the outer surface of each test article prior to testing. Strain gages were applied at select locations to monitor stress concentrations and buckling behavior. Typical strain gage patterns are shown in Fig. 7. In addition, one section of each specimen was painted with a black and white speckle pattern so that a Vision Image Correlation (VIC)[17] system could be used to monitor full-field displacements and strains over the taper and fitting region on one end of each strut, as shown for specimen N-H-1 in Fig. 8.

Strut N-H-3 was fabricated with Teflon inserts to simulate manufacturing-induced delaminations that may not be detected. These inserts were placed at selected locations through the thickness and along the length. The location of these inserts is shown in Fig. 9 where the color of the squares indicating the Teflon inserts indicates the location through the thickness, with green being the closest to the outer surface, blue being the closest to the inner surface and red being in the center of the stacking sequence. Strut N-H-3 was also subjected to impact damage prior to loading. The impact was inflicted using a drop weight impactor with a 25 lb weight with a 1-inch diameter tup. Trial impacts of 40, 80 and 100 ft-lb were inflicted to strut N-H-1 after it was failed to determine the impact energy to use on strut N-H-3. A photograph of the results of these trials is shown in Fig. 10. Since the 100 ft-lb impact resulted in minimal visible damage, this level was selected for impact to strut N-H-3. A photograph of the pre-test damage to strut N-H-3 is shown in Fig. 11.

Each test article was mounted vertically between fixtures and a load applied through the threaded end fittings. Photographs of the test arrangements are shown in Fig. 8. In each case, the strut fitting at the top was attached to brackets which attached to a rigid backstop. The test fixtures at the top and bottom were designed to allow for rotation in any direction during the testing as described in reference 15. For the heavily loaded struts, the fitting at the bottom of the strut attached to a 225 kip load cell, which was attached to a 225 kip actuator which was attached to the backstop and supported by the floor. For the lightly loaded struts, the fitting at the bottom was attached to a 10 kip load cell. Load was applied through a hand pump hydraulic actuator. More details of the testing arrangement and set-up are presented in reference 15.

Struts were loaded in tension alone, compression alone or tension followed by compression. Heavily loaded struts were loaded at a rate of 0.001 in/sec in either tension or compression until the desired load or failure was reached. Pristine struts N-H-1 and N-H-2 were loaded to DLL in tension then to their maximum loading in compression. Strut B-H-1 was loaded to DLL in tension and then to failure in compression. Strut B-H-2 was loaded only to failure in compression. Strut N-H-3 was loaded to its maximum load in compression. Strut N-L-1 was loaded to 2 times its DUL in tension and then to its maximum load in compression. Strut N-L-2 was loaded to its maximum load in compression.

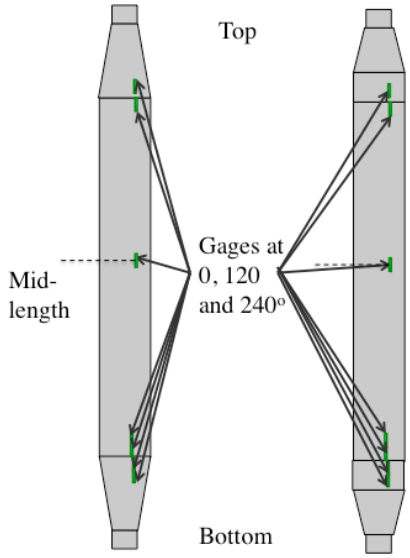

Figure 7. Typical strain gage pattern.

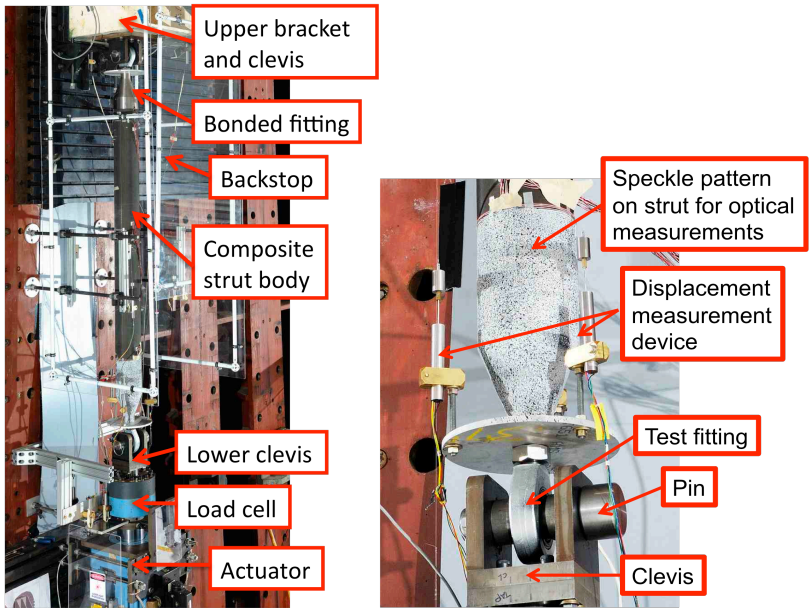

Figure 8. Strut B-H-1 in the test fixture prior to testing.

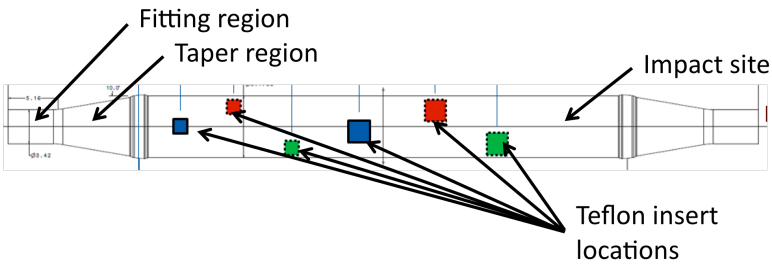

Figure 9. Location of inserts and damage for strut N-H-3.

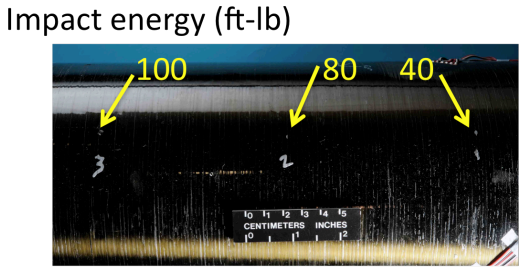

Figure 10. Trial impacts.

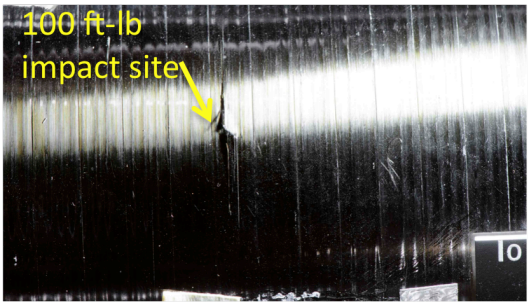

Figure 11. Impact damage on strut N-H-3.

The behavior of each test article was monitored by numerous linearly variable displacement transducers (LVDT). Three LVDTs placed at 0, 120, and 240 degrees around the circumference of the strut measured axial lengthening or shortening of the entire strut; one LVDT measured the axial displacement of the constant-cross section region of the composite body, and two LVDTs at 0 and 90 degrees around the circumference measured radial motion at the midlength of the strut. Strain gage data, LVDT data, and VIC images of the lower region of each specimen were recorded at the rate of 1 Hz.

V. Results and Discussion

A summary of the displacements, strains and failure modes for the seven test articles is presented herein, and these results are compared to analytical predictions. Predicted and experimental maximum compression loads are shown in Table 5.

Table 5. Strut loads.

Strut ID	Design Requirement (lb)	Predicted Maximum Load (lb)	Experimental Maximum Load (lb)
B-H-1	107,585	113,804	43,500
B-H-2	107,585	113,804	79,900
N-H-1	107,585	129,998	119,300
N-H-2	107,585	129,998	121,700
N-H-3	107,585	not analyzed	21,100
N-L-1	1,183	1,290	2180
N-L-2	1,183	1,290	1980

A. Loads and Displacements

1. Heavily loaded struts

The heavily loaded bonded-fitting struts did not support the required loads. The first bonded-fitting strut tested, B-H-1, sustained damage in the initial tensile loading to DLL so it only sustained approximately 43,000 lb in the subsequent compressive loading. In order to start with a pristine strut for compression loading, the second bonded-fitting strut, B-H-2, was not initially loaded in tension. Even without the preload, strut B-H-2 failed in compression at approximately 80,000 lb, or approximately DLL. Little warning of impending failure was evident in the global measure of displacement. The end-shortening versus load for the compressive loadings are shown in Fig. 12. Strut B-H-1 measurements are shown as blue dashed lines for the three measurement locations around the circumference. Strut B-H-2 measurements are shown as dashed red lines while the analytical prediction is shown as the solid black line.

The three measurements for each strut agree well with each other and with analysis, indicating no buckling behavior is occurring in either strut and the struts have similar global stiffnesses.

The radial deflections measured at two points at the midlength of each strut can be used to evaluate out-of-plane motion. These measurements for struts B-H-1 and B-H-2 are shown in Fig. 13 as blue and red lines, respectively. Since both of these measurements remain less than 0.02 inches, there was probably no buckle prior to failure.

Both heavily loaded pristine struts with corrugated fittings withstood their tensile DLL prior to compressive loading. Under compressive loading, one heavily loaded pristine corrugated-fitting strut withstood 110% of DUL while the other withstood 112% of DUL. All evidence of failure was in the fitting region. The end-shortening versus load for the compressive loadings are shown in Fig. 14. Strut N-H-1 measurements are shown as blue dashed lines for the three measurement locations around the circumference. Strut N-H-2 measurements are shown as dashed red lines while the analytical prediction is shown as the solid black line. The three measurements for each strut agree well with each other and with analysis for load less than 108,000 lb indicating no buckling behavior is occurring in either strut prior to DUL and the struts have similar global stiffnesses.

The average of the three axial displacement measurements for all three N-H struts are presented in Fig. 15. The impact-damaged strut, N-H-3, failed through the impact site at a load of 21,100 lb. The initial stiffness of this strut was the same as N-H-1 and N-H-2 but this damage, though not readily visible without the right lighting, caused severe enough damage to reduce the failure load by 80 percent.

The radial deflection measured on two points at the midlength of each strut can be used to evaluate the out-of-plane motion of each strut. These measurements for struts N-H-1 and N-H-2 are shown in Fig. 16 as blue and red lines, respectively. Since both of these measurements are very small until immediately prior to failure, these struts did not buckle prior to failure.

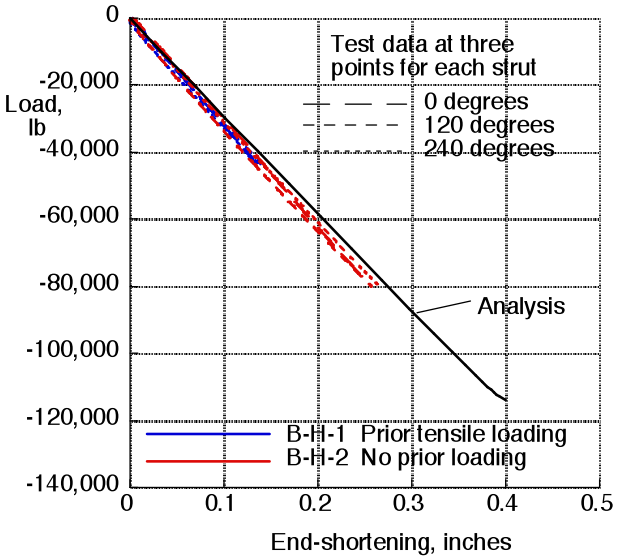

Figure 12. Axial displacement for struts of type B-H.

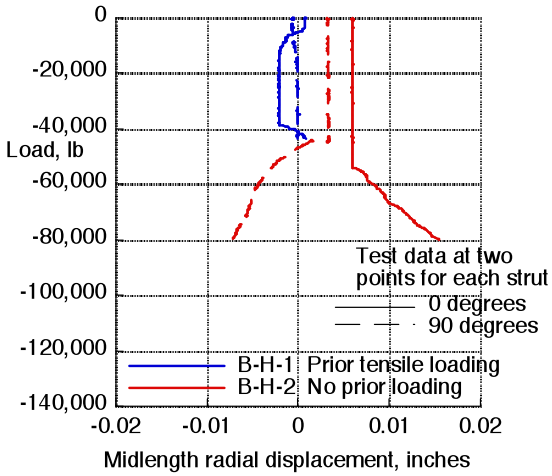

Figure 13. Radial displacement for struts of type B-H.

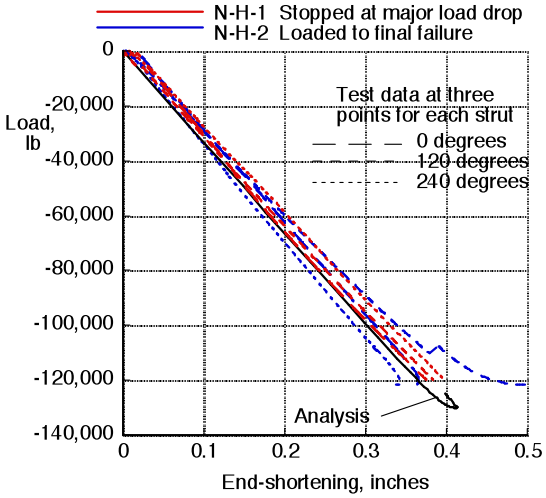

Figure 14. Axial displacement for pristine struts of type N-H.

2. Lightly loaded struts

The lightly loaded struts withstood the applied tensile and compressive loading with no visible damage but buckled at their maximum loading. Strut N-L-1 was loaded to two times its DUL in tension then loaded in compression to its maximum (buckling) load. Its maximum load was approximately 2.0 times the predicted maximum compressive load. Strut N-L-2 was not preloaded in tension but only loaded in compression and supported approximately 1.6 times its predicted maximum load in compression. Both of the lightly loaded struts supported more than DUL in compression.

The average of the axial displacement measurements for specimens N-L-1 and N-L-2 are shown as the green lines in Fig. 17. Analytical predictions are shown as back lines. The strut motion is not uniform around the circumference, however, the measurements are repeatable from one strut to the next. In both cases, good agreement between an average of the three test measurements (shown as the solid green lines) and the analysis can be seen for the initial loading of the struts. The struts buckled at a greater load than predicted by the analysis, possibly indicating that the influence of the initial geometric imperfection may not have been as significant as anticipated or that there may have been friction or other behavior at the ends in the fixtures to invalidate the "pinned" assumption at the ends. The full-field axial motion obtained from the vision image correlation system for a load level just prior to failure of 2,187 lb for strut N-L-1 is also shown in Fig. 17 for the bottom 10 inches of the strut. A relatively uniform axial deformation is seen. Note that the white regions in the figure represent areas for which the strain could not be calculated, typically because of surface obstructions or shadow.

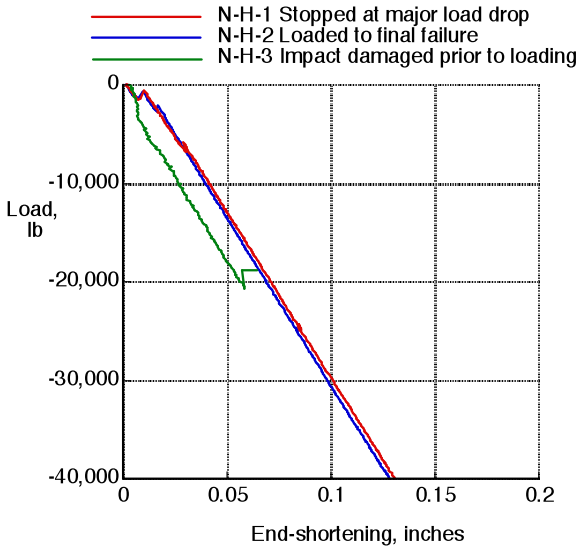

Figure 15. Average axial displacement for struts of type N-H.

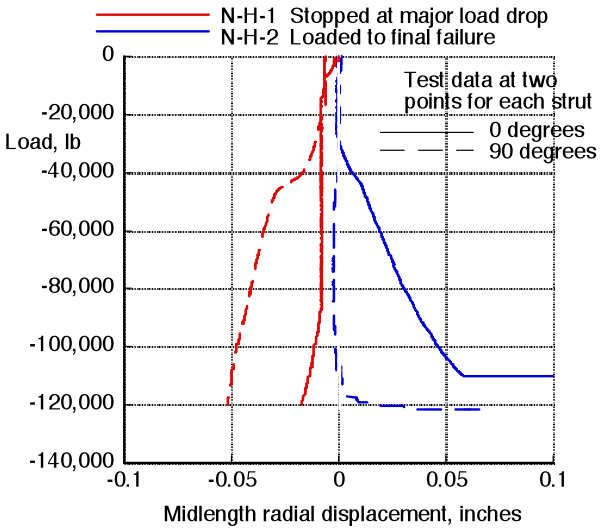

Figure 16. Radial displacement for struts of type N-H.

The radial deflection measured on two points at the midlength of each strut can be used to evaluate the out-of-plane motion of each strut. These measurements for struts N-L-1 and N-L-2 are shown in Fig. 18 as blue and red lines, respectively. Radial motion indicates buckling occurred for both struts at a similar load of approximately 2000 lb and in a similar direction. Applied axial displacement was continued beyond the initial buckling point so the radial deflection curves can be seen to flatten out where the increased axial displacement supported no additional load. The full field measurements at a load just prior to failure for strut N-L-1 in the directions parallel to and perpendicular to the backstop are also shown in Fig. 18. As the strut buckles, this lower 10-inch region of the strut moves less than 0.1 inches parallel to the test wall (top fringe plot) and up to 0.5 inches toward the test wall (bottom fringe plot) as it buckles.

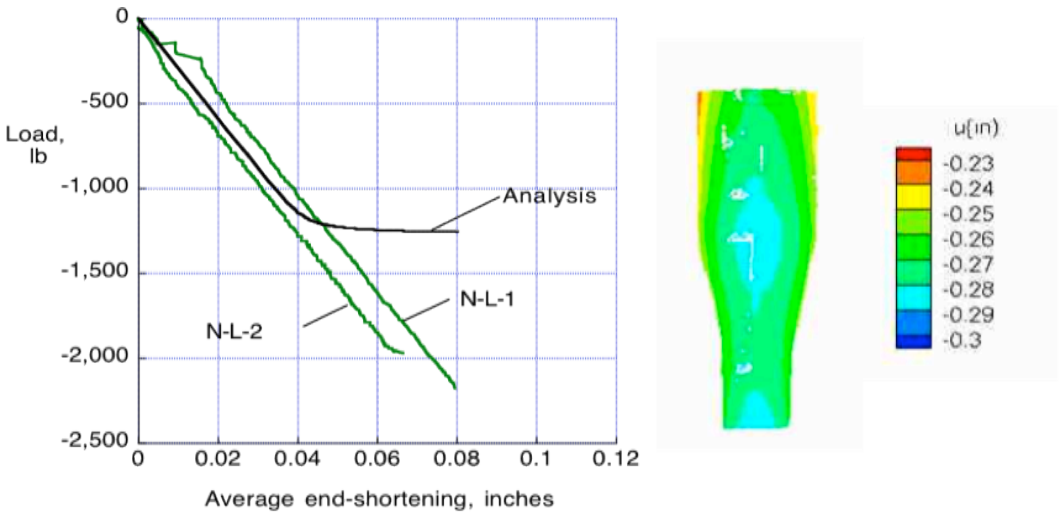

Figure 17. Axial displacement for struts of type N-L with full field displacement at a load of 2,187 lb.

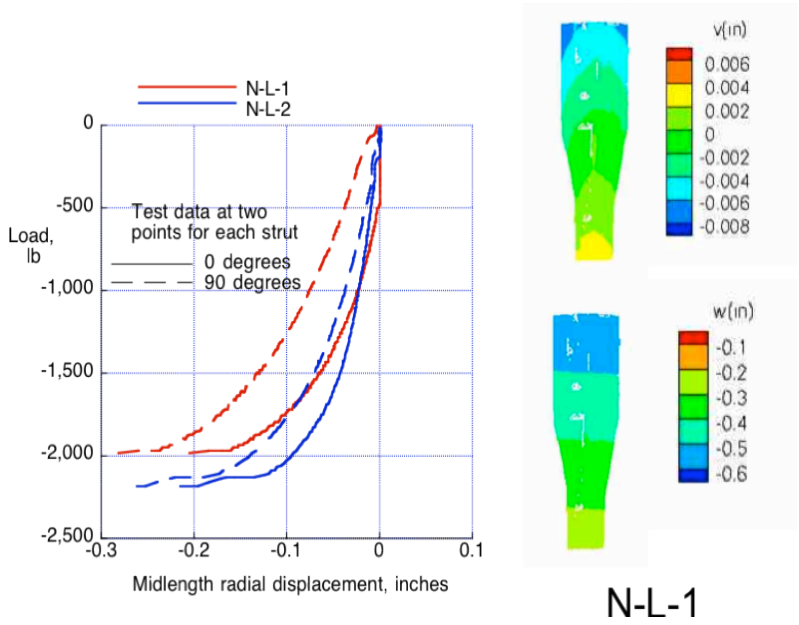

Figure 18. Radial displacement for struts of type N-L with full field displacement at a load of 2,187 lb.

B. Strain

1. *Heavily loaded struts*

Midlength axial strains for specimens B-H-1 and B-H-2 are shown in red and blue, respectively, in Fig. 19. Midlength axial strains for specimens N-H-1 and N-H-2 are shown in red and blue, respectively, in Fig. 20. Measured axial strains at three locations around the circumference are shown as three dashed lines of different dash lengths in Figs. 19 and 20. Midlength strains for struts B-H are linear to failure and consistent between the two struts and around the circumference. Midlength strains for struts N-H are linear until immediately prior to failure and are also consistent between the two struts and around the circumference.

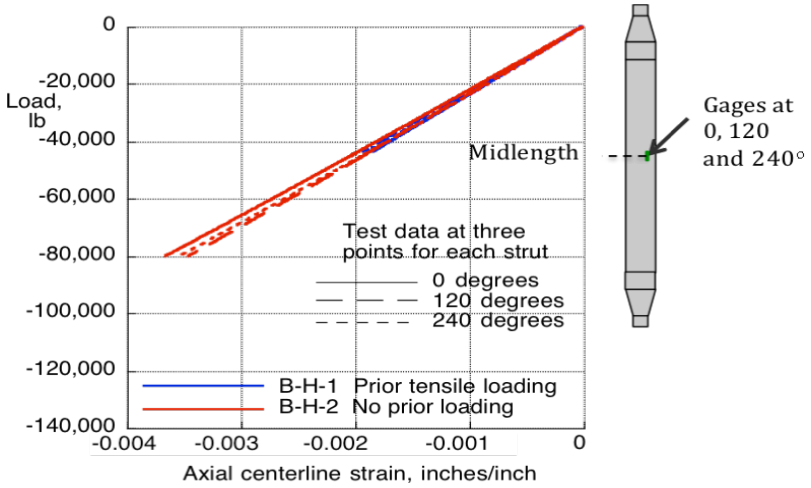

Figure 19. Axial strain midlength for struts of type B-H.

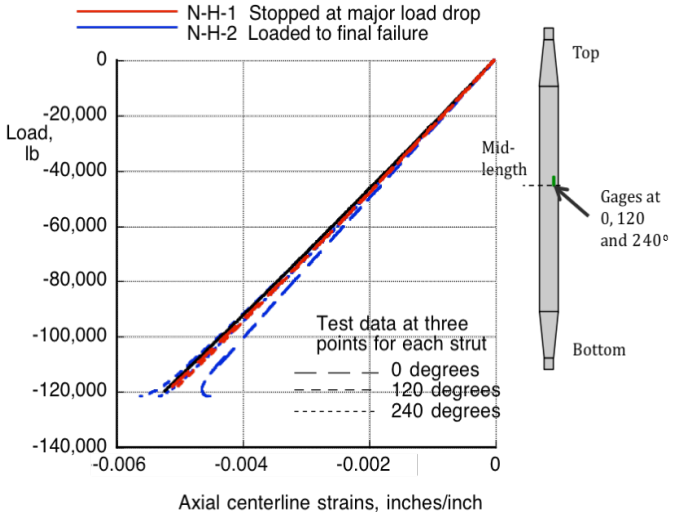

Figure 20. Axial strain midlength for struts of type N-H.

Measured axial strains at the fitting-to-composite interface region for specimens B-H-1 are shown in Fig. 21 for the tensile loading and Fig. 22 for the subsequent compressive loading. The full-field axial strain for the lower end of strut B-H-1 at approximately 43,835 lb tensile load and 43,615 lb compressive load are shown in Figs. 21 and 22, respectively. Axial gages were located on the exterior surface of the composite body and on the exterior surface of the titanium fitting at three locations around the circumference. Strains on the composite are shown in red and strains on the titanium surface are shown in blue. The discontinuities in the measured strain under tensile loading are believed to indicate damage to the bond between the composite steps and the titanium fitting. Damage to the bond began to initiate at a load significantly less than DLL in the tensile loading.

The strains at the interface between the composite and the titanium fitting are shown in Fig. 23 for strut B-H-2 loaded in compression. The full field strain for strut B-H-II-2 at approximately 79,800 lb compressive load is shown in figure 23. The strains in the titanium are not the same as in the composite body, however, both are linear and consistent around the circumference.

The strains on the composite surface in the taper region of strut N-H-2 are shown in Fig. 24. The red lines represent strains in the uniform diameter region adjacent to the taper and the blue lines represent strains in the taper itself. The strains are not uniform around the circumference, but all remain linear for load less than DUL. Nonlinearities can be seen in the strains in the taper region for load greater than DUL which could represent a failure in the adhesive bond between the carbon-epoxy and the titanium fitting.

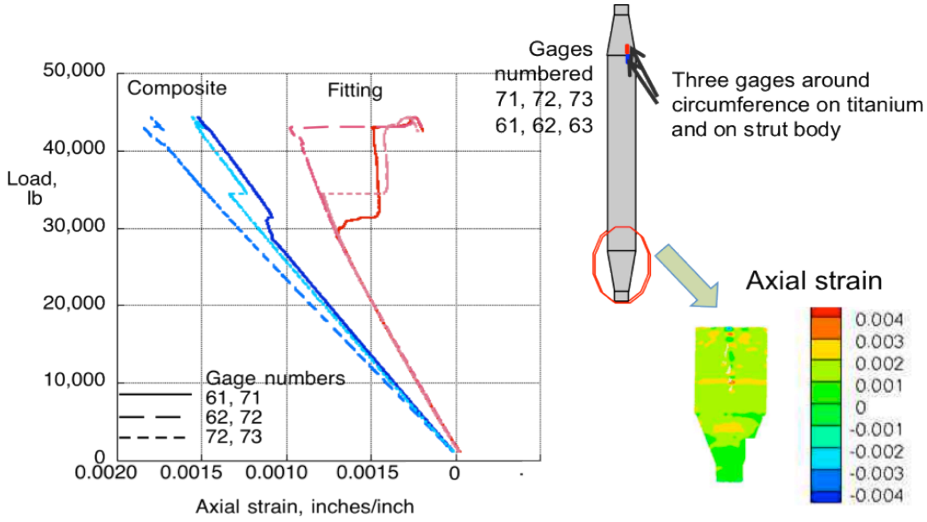

Figure 21. Axial strain for interface location for strut B-H-1 loaded in tension with full field strain at a load of 43,835 lb.

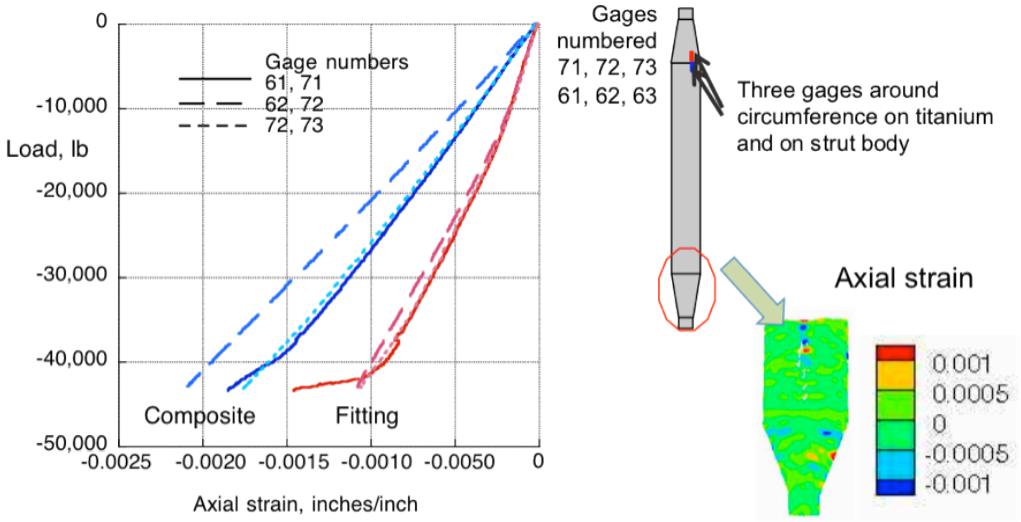

Figure 22. Axial strain at interface location for strut B-H-1 loaded in compression with full field strain at a load of 43,615 lb.

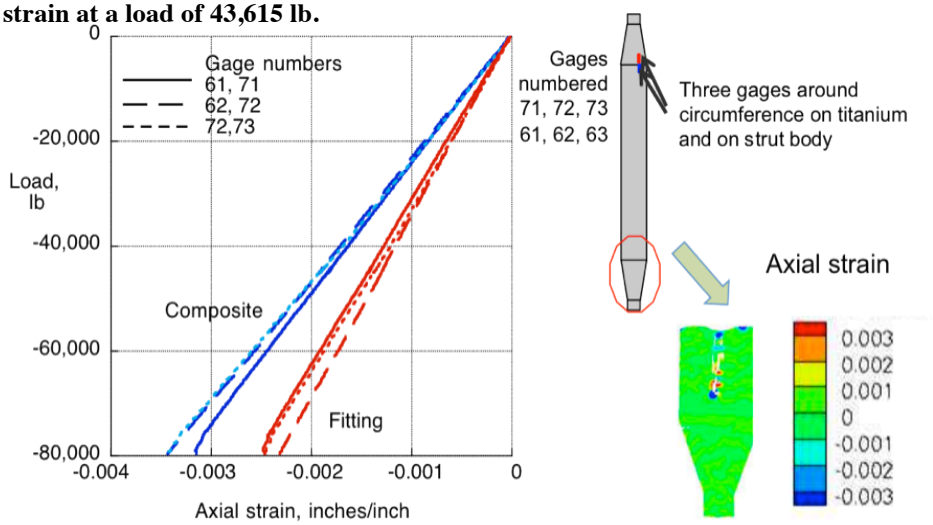

Figure 23. Axial strain at interface location for strut B-H-2 loaded in compression with a full field strain of 79,980 lb.

The bending strain can be determined by averaging the strains measured at the midlength location and then subtracting this value from each measured value. This calculation removes the axial component of the strain, leaving only the bending component. The bending component at the three circumferential locations for strut N-H-2 is shown in Fig. 25. The bending strain is less than 10 percent of the total strain, also shown in the figure. Struts B-H did not display bending behavior.

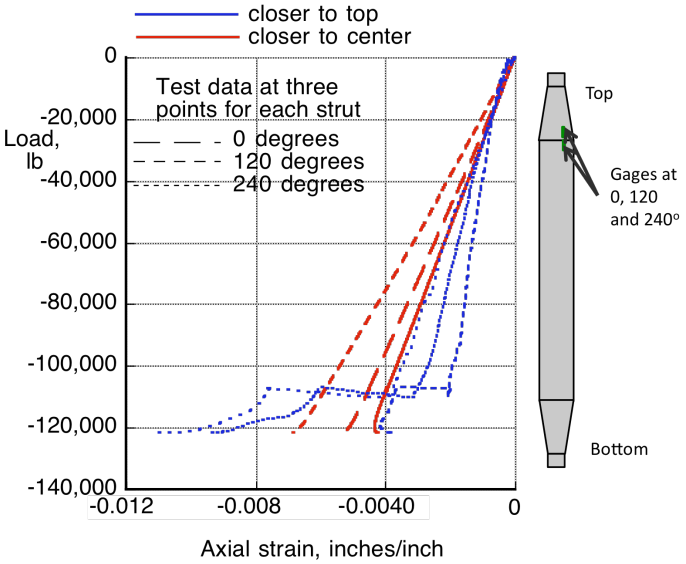

Figure 24. Axial strain at taper for struts of type N-H-2.

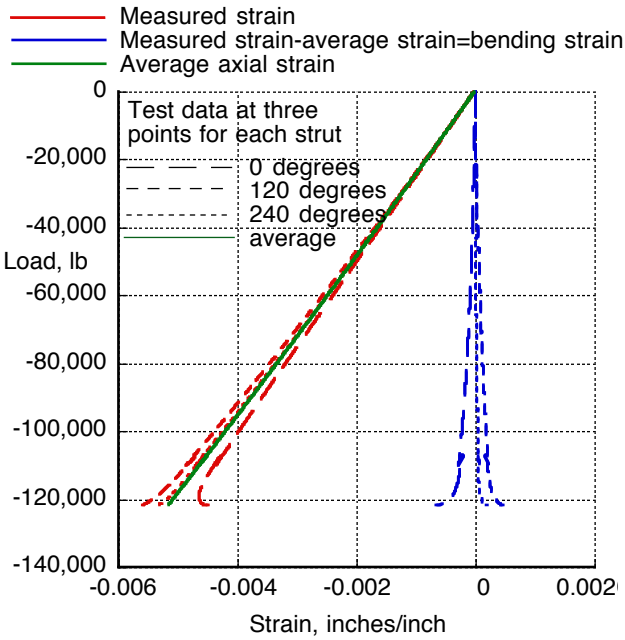

Figure 25. Bending strain for strut N-H-2.

2. Lightly loaded struts

Midlength axial strains for specimens N-L-1 and N-L-2 are shown in blue and red, respectively, in Fig. 26. Measured axial strains at three locations around the circumference are shown as three dashed lines of different dash lengths. Midlength strains for struts N-L show evidence of buckling well before failure, consistent with the displacement results.

The strains on the composite surface in the uniform diameter region near the taper region and in the taper region itself of struts N-L-1 and N-L-2 are shown in Fig. 27. The red lines represent strains in the uniform diameter region adjacent to the taper and the blue lines represent strains in the taper itself. The strains in the uniform diameter region are uniform around the circumference and consistent between the two struts until immediately before failure. Nonlinearities can be seen in the strains in the taper region for the full loading range suggesting a redistribution of load in the corrugations as load is increased.

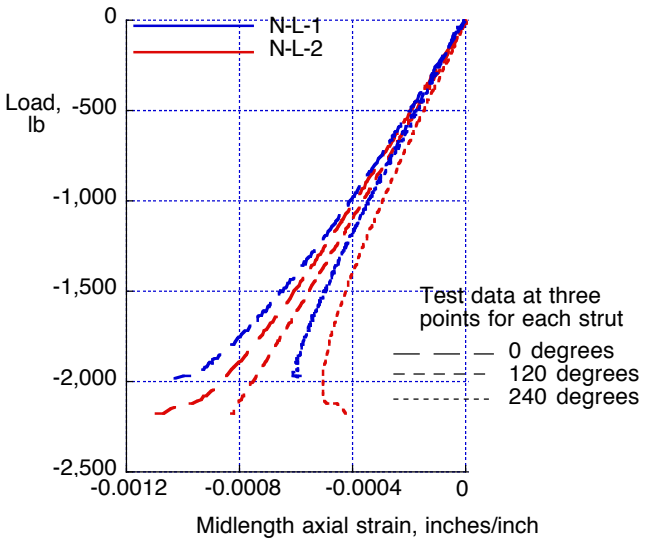

Figure 26. Midlength strain for lightly loaded struts.

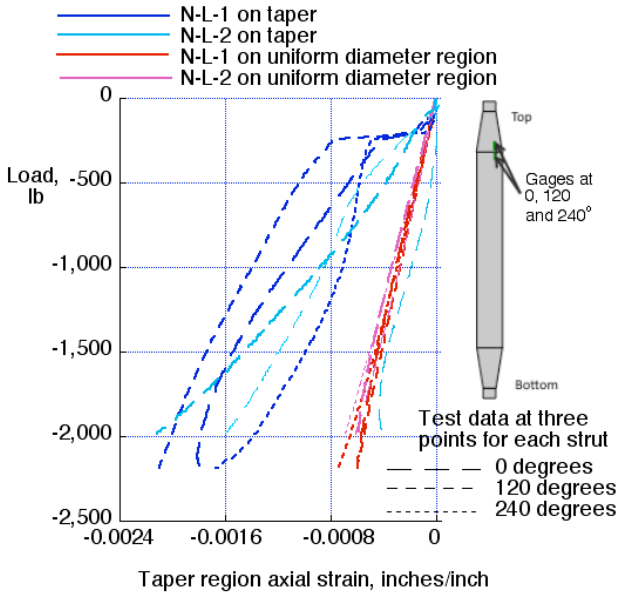

Figure 27. Strain in taper region of struts of type N-L.

The bending component at the three circumferential locations for strut N-L-1 is shown in Fig. 28. The bending strain is small for low loads but up to approximately 50 percent of the total strains as the loading is approaching the buckling load. The nonlinear region of the curves represents post-buckling behavior, where bending strain has the largest magnitude.

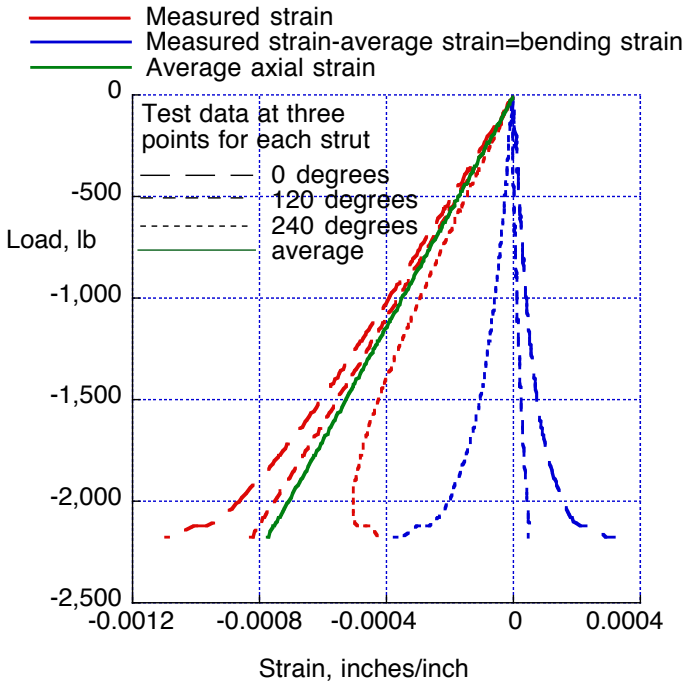

Figure 28. Measured and bending strains for strut N-L-1.

C. Failure

Photographs of failed heavily loaded specimens are shown in Figs. 29 and 30. Both struts with the bonded end fittings failed the composite-to-fitting joint as shown in Fig. 29. The failure of the bond was evident around the entire circumference of the strut. Despite the fact that the bond area was maximized by locating it in the maximum diameter region of the strut, the adhesive bond did not sustain the required load. Visible failures in the corrugated-fitting struts were generally in the fitting region and of the type shown in

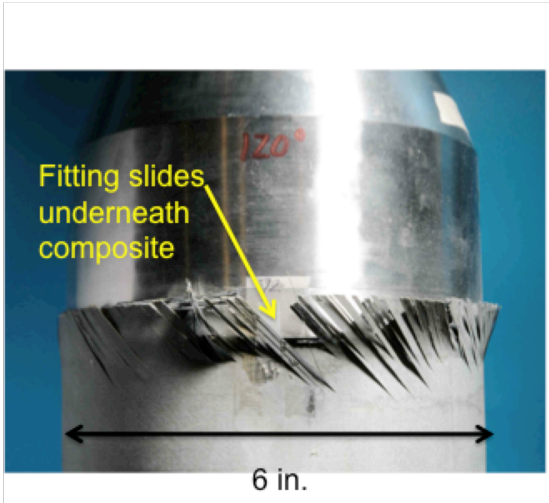

Fig. 29. Failure of a bonded fitting strut.

Fig 30. Failure of a corrugated fitting strut.

figure 30 but not all struts displayed visible failure. Failure of the corrugated fitting struts were all at loads greater than DUL. Lightly loaded specimens buckled when they reached their maximum load and left little evidence of fiber damage after loading was removed. Photographs of strut N-L-2 showing its buckling at its maximum loading are shown in Fig. 31. A summary of these failures is presented in Table 6. NDE was not conducted after test to find any non-visible damage.

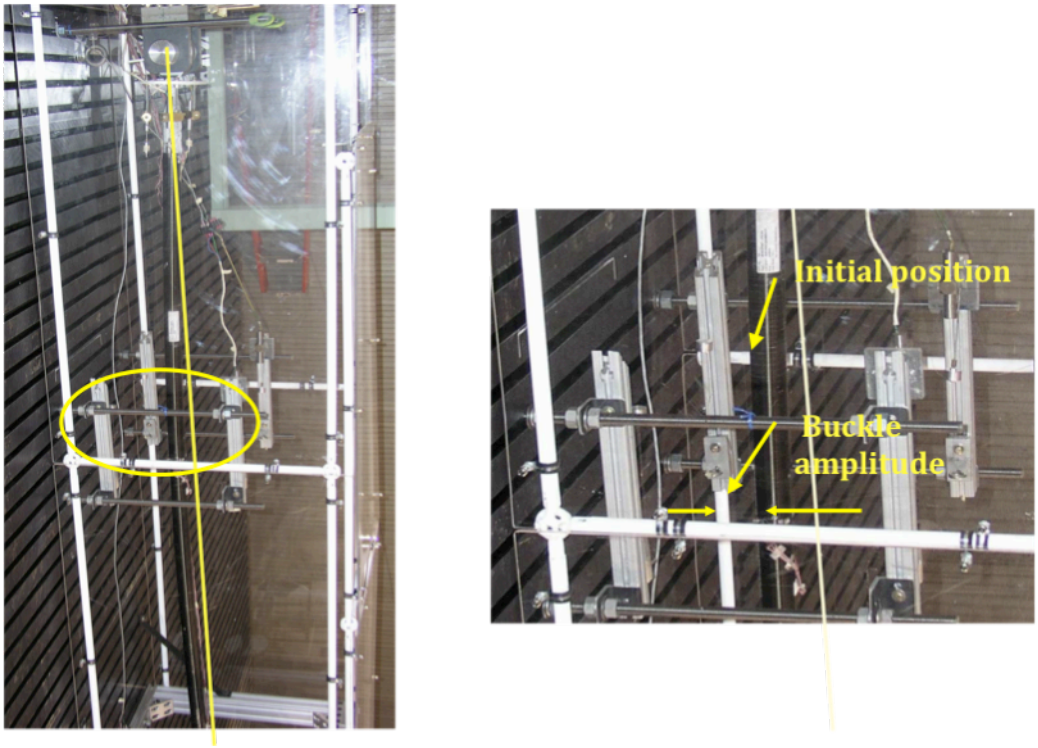

Figure 31. Buckling of strut N-L-1 under maximum loading.

Table 6. Failure mode of tested struts.

Strut ID	Failure mode
N-H-1 and N-H-2	Overwrap plies in fitting area
N-H-3	Along length and around circumference through impact site
N-L-1 and N-L-2	Buckling, no significant visible strength failure
B-H-1 and B-H-2	Failure of bond between fitting and composite

X. Application to Altair Lunar Lander

Before this study was initiated, a great deal of work had been performed in examining lightly loaded struts but not as much in highly loaded struts. Design, analysis and testing had not been sufficient to have confidence that highly loaded composite struts were a feasible choice for the structure for the Altair lunar lander. For this reason, the technology readiness level (TRL)[18] was assumed to be at a level of 4 based on the work on more lightly loaded struts for other applications. This study involved full-scale struts loaded to the maximum required uniaxial loading. In this study, a strut concept was proven to meet the loading requirements in both tension and compression. The design, analysis, and testing effort in this study demonstrated that the strut-based design is a viable concept. However, since no thermal or vibration conditions have been examined, as would be necessary to simulate a space and launch environment, the

TRL has only been raised to 5. Further studies involving temperature extremes appropriate for orbit and long-term lunar exposure and vibrations similar to those anticipated on launch would be required to raise the TRL to 6.

XI. Concluding Remarks

Composite struts were designed with the objective of meeting the loading requirements for the most heavily loaded and the most lightly loaded struts for the Altair lunar lander. Seven minimum-weight carbon-epoxy struts were fabricated and experimentally evaluated through uniaxial loading. All struts contained titanium end fittings. Five struts were fabricated with a tapered composite body and a corrugated end fitting where carbon fibers were wrapped around the corrugations to provide a mechanical connection between the fitting and the carbon-epoxy body of the strut. Two struts were fabricated using an adhesively bonded step lap joint between the carbon-epoxy body of the strut and the end fitting. The fittings were tapered in the struts with the step lap joint so the composite body could have a uniform diameter. Uniaxial tension and compression loading was applied to each type of strut to determine their strain, displacement, buckling and failure characteristics.

Struts fabricated using the corrugated-fitting concept met the required compressive loading for heavily and lightly loaded struts. Heavily loaded struts of this type did not buckle and displayed failures in the fitting region where failures could be seen. Lightly loaded struts buckled into a single half-wave and displayed no evidence of strength failures. However, struts fabricated using the bonded-fitting concept failed at significantly lower loads than the design requirement. Damage to the bond began to initiate at a load significantly less than DLL in the tensile loading. Neither bonded fitting strut sustained load greater than DLL. A bonded joint depending only on the adhesive might be a viable concept but the struts in this study did not support the required load. Both bonded-fitting struts failed at the adhesive bond between the titanium and composite. Only the corrugated-fitting struts evaluated in this study meet the requirements defined by the Altair lunar lander project. In addition, one severely impact-damaged heavily loaded strut sustained barely visible damage but failed through the impact site at a load of approximately 20 percent of the failure load of the nominally identical pristine struts.

These results indicate that the use of highly loaded struts for a lander design carrying heavy loads through the primary structure during launch is feasible. As with any design, significant validation testing would be required. Because highly loaded struts tested here failed in the region of the end fittings, it is reasonable to suggest that end-fitting design may be a key area in the design of heavily loaded struts for Altair-type applications. The fitting-to-composite joints are critical both because it is a challenge to achieve sufficient strength at the tube-fitting interface, and because the mass of the joint may be a significant portion of the total strut assembly, reducing the mass benefit advantage of utilizing a truss-based design.

References

1. Wagner, H., "Remarks on Airplane Struts and Girders under Compressive and Bending Stresses. Index Values." NACA TM 500. 1929.

2. Dow, N. F., and Hickman, W. A., "Design Charts for Flat Compression Panels Having Longitudinal Extruded Y-Section Stiffeners and Comparison with Panels Having Formed Z-Section Stiffeners," NACA NT 1389, 1947.

3. Williams, J., Anderson, M., Rhodes, M., Starnes, J., and Stroud, J., "Recent Developments in the Design, Testing and Impact-Damage Tolerance of Stiffened Composite Panels," NASA TM 80077, 1979.

4. Williams, J. G., and Stein, M., "Buckling Behavior and Structural Efficiency of Open-Section Stiffened Composite Compression Panels." *AIAA Journal,* Vol. 14, No. 11, 1976, pp. 1618-1626.

5. Williams, J. G., and Mikulas, M. M., Jr. "Analytical and Experimental Study of Structurally Efficient Composite Hat-Stiffened Panels. Presented at the ASME/AIAA SAE 16th Structures, Structural Dynamics and Materials Conference, Denver Colorado, 1995. AIAA Paper No. 75-754.

6. Dow, N. F., and Rosen, B. W., "Structural Efficiency of Orthotropic Cylindrical Shells Subjected to Axial Compression," *AIAA Journal*, Vol. 4, No 3, 1966, pp. 481-485.

7. Haynie, W. T., and Hilburger, M., "Comparison of Methods to Predict Lower Bound Buckling Loads of Cylinders Under Axial Compression," Presented at the 51st AIAA/ASME/ASCE/AHS/ASC Structures, Structural Dynamics, and Materials Conference, 2010, Orlando, Florida, AIAA Paper No 2010-2532.

8. Constellation Program: America's Spacecraft for a New Generation of Explorers, The Altair Lunar Lander. NASA facts, Lyndon B. Johnson Space Center, 2008.

9. Brewster, Jebediah, Design of Structurally Efficient Tapered Struts NASA CR 2009-8393, December 2009.

10. Messinger, R., "Design of Structurally Efficient Tapered Struts," NASA CR 2010-216698, 2010.

11. Deo, R., Benner, H., Dawson, V., Olason, E., and Harrison, R. "Design of Structurally Efficient Tapered Struts (SETS)." NASA CR 2010-216699.

12. Messinger, R., "Design and Manufacturer of Structurally Efficient Composite Struts – Concept 1," Final report for NASA contract NAS1-NNL04AA11B Task NNL09AC35T, 2009.

13. Pires, K., Benner, H., Deo, R., Grover, R., Palm, T., McLaughlin, M., Olason, E., Lucking, R., and Collier, C., "Design and Manufacturer of Structurally Efficient Composite Struts – Concept 2," Final report for NASA contract NAS1-NNL04AA13B Task NNL09AC36T, 2010.

14. Jegley, D., Wu, K., Phelps, J, McKenney, M., and Oremont, L., "Structural Efficiency of Composite Struts for Aerospace Application," AIAA paper 925421 presented at the 52nd AIAA/ASME/ASCE/AHS/ASC Structures, Structural Dynamics and Materials Conference, Denver CO, 2011.

15. Wu, K., Phelps, J, McKenney, M., and Jegley, D., "Highly Loaded Composite Strut Test Development," AIAA paper 932820 presented at the 52nd AIAA/ASME/ASCE/AHS/ASC Structures, Structural Dynamics and Materials Conference, Denver CO, 2011.

16. ABAQUS version 6.9 EF1 On-line Documentation, ABAQUS Analysis User's Manual, Dassault Systemes Simulia Corp., Providence, RI, 2009.

17. McGowan, David M., Ambur, Damodar R., and McNeil, Stephen R., "Full-field Structural Response of Composite Structures: Analysis and Experiment," presented at the 44th AIAA/ASME/ASCE/AHS Structures, Dynamics and Materials Conference, AIAA 2003-1623, Norfolk, VA, April 2003.

18. Mankins, John C., "Technology Readiness Levels, A White Paper," April 6, 1995.

REPORT DOCUMENTATION PAGE

Form Approved
OMB No. 0704-0188

1. REPORT DATE *(DD-MM-YYYY)*	2. REPORT TYPE	3. DATES COVERED *(From - To)*
01- 02 - 2011	Technical Memorandum	

4. TITLE AND SUBTITLE
Evaluation of Long Composite Struts

5a. CONTRACT NUMBER

5b. GRANT NUMBER

5c. PROGRAM ELEMENT NUMBER

6. AUTHOR(S)
Jegley, Dawn C; Wu, K. Chauncey; Phelps, James E.; McKenney, Martin J.; Oremont, Leonard; Barnard, Ansley

5d. PROJECT NUMBER

5e. TASK NUMBER

5f. WORK UNIT NUMBER
727950.04.05.23

7. PERFORMING ORGANIZATION NAME(S) AND ADDRESS(ES)
NASA Langley Research Center
Hampton, VA 23681-2199

8. PERFORMING ORGANIZATION REPORT NUMBER
L-19983

9. SPONSORING/MONITORING AGENCY NAME(S) AND ADDRESS(ES)
National Aeronautics and Space Administration
Washington, DC 20546-0001

10. SPONSOR/MONITOR'S ACRONYM(S)
NASA

11. SPONSOR/MONITOR'S REPORT NUMBER(S)
NASA/TM-2011-217049

12. DISTRIBUTION/AVAILABILITY STATEMENT
Unclassified - Unlimited
Subject Category 39
Availability: NASA CASI (443) 757-5802

13. SUPPLEMENTARY NOTES

14. ABSTRACT
Carbon-epoxy tapered struts are structurally efficient and offer opportunities for weight savings on aircraft and spacecraft structures. Seven composite struts were designed, fabricated and experimentally evaluated through uniaxial loading. The design requirements, analytical predictions and experimental results are presented. Struts with a tapered composite body and corrugated titanium end fittings successfully supported their design ultimate loads with no evidence of failure.

15. SUBJECT TERMS
Composites; Bonded joint; Buckling; Carbon-epoxy; Corrugated fitting; Graphite; Lunar lander

16. SECURITY CLASSIFICATION OF:			17. LIMITATION OF ABSTRACT	18. NUMBER OF PAGES	19a. NAME OF RESPONSIBLE PERSON
a. REPORT	b. ABSTRACT	c. THIS PAGE			STI Help Desk (email: help@sti.nasa.gov)
					19b. TELEPHONE NUMBER *(Include area code)*
U	U	U	UU	22	(443) 757-5802